SARM1-specific motifs in the TIR domain enable NAD$^+$ loss and regulate injury-induced SARM1 activation

Daniel W. Summers[a,b], Daniel A. Gibson[b], Aaron DiAntonio[b,c,1], and Jeffrey Milbrandt[a,c,1]

[a]Department of Genetics, Washington University in St. Louis, St. Louis, MO 63110; [b]Department of Developmental Biology, Washington University in St. Louis, St. Louis, MO 63110; and [c]Hope Center for Neurological Disorders, Washington University in St. Louis, St. Louis, MO 63110

Edited by Richard H. Goodman, Vollum Institute, Portland, OR, and approved August 19, 2016 (received for review January 27, 2016)

Axon injury in response to trauma or disease stimulates a self-destruction program that promotes the localized clearance of damaged axon segments. Sterile alpha and Toll/interleukin receptor (TIR) motif-containing protein 1 (SARM1) is an evolutionarily conserved executioner of this degeneration cascade, also known as Wallerian degeneration; however, the mechanism of SARM1-dependent neuronal destruction is still obscure. SARM1 possesses a TIR domain that is necessary for SARM1 activity. In other proteins, dimerized TIR domains serve as scaffolds for innate immune signaling. In contrast, dimerization of the SARM1 TIR domain promotes consumption of the essential metabolite NAD$^+$ and induces neuronal destruction. This activity is unique to the SARM1 TIR domain, yet the structural elements that enable this activity are unknown. In this study, we identify fundamental properties of the SARM1 TIR domain that promote NAD$^+$ loss and axon degeneration. Dimerization of the TIR domain from the *Caenorhabditis elegans* SARM1 ortholog TIR-1 leads to NAD$^+$ loss and neuronal death, indicating these activities are an evolutionarily conserved feature of SARM1 function. Detailed analysis of sequence homology identifies canonical TIR motifs as well as a SARM1-specific (SS) loop that are required for NAD$^+$ loss and axon degeneration. Furthermore, we identify a residue in the SARM1 BB loop that is dispensable for TIR activity yet required for injury-induced activation of full-length SARM1, suggesting that SARM1 function requires multidomain interactions. Indeed, we identify a physical interaction between the autoinhibitory N terminus and the TIR domain of SARM1, revealing a previously unrecognized direct connection between these domains that we propose mediates autoinhibition and activation upon injury.

SARM | NAD | cell death | axon degeneration | sarmoptosis

Axon degeneration in response to injury or disease is a hallmark of neurological disorders of the peripheral and central nervous systems. Akin to programmed cell death pathways, such as apoptosis, axon injury in response to disease or trauma stimulates a local signaling cascade that executes destruction of the injured axon segment (1). Despite growing attention, the molecular details of this prodegenerative cascade are still unclear. A more substantial understanding of the molecular factors that participate in this axon destructive process will likely provide new therapeutic strategies for peripheral neuropathies and other neurodegenerative conditions.

Genetic screens in invertebrate and vertebrate model systems identified the Sterile alpha and Toll/interleukin receptor (TIR) motif-containing protein 1 (SARM1) as a conserved, fundamental executioner of pathological axon destruction (2, 3). After nerve injury, SARM1 is required for the precipitous loss of the metabolite NAD$^+$ (4). Augmenting NAD$^+$ biosynthetic pathways protects injured axons from degeneration, suggesting this step is crucial in axonal breakdown (5, 6). In addition to local axon degeneration, SARM1 promotes neuronal cell death in response to mitochondrial toxins, oxygen glucose deprivation, and viral infection (7–10). Activated SARM1 can induce cell death independent of other known programmed cell death programs in a pathway termed sarmoptosis. Hence, SARM1 exerts a major role in pathological neuron destruction, so a deeper understanding of the molecular mechanism of SARM1 function may identify novel targets for the inhibition of this prodestructive factor.

Domain analysis of the SARM1 protein generated a model of SARM1 activation and function (3, 11, 12). SARM1 possesses a Toll/interleukin receptor (TIR) domain that is required for SARM1-dependent axon degeneration and cell death. Recently, others and we demonstrated that enforced dimerization of the SARM1 TIR domain is sufficient to induce local axon degeneration (3, 4, 13). Tandem sterile alpha motif (SAM) domains mediate SARM1 multimerization, and hence are required for SARM1 activity. The SARM1 N-terminal domain contains Heat/Armadillo repeats and restrains SAM-TIR activity, maintaining SARM1 in an autoinhibited state (3, 11, 12). Although SARM1 could possess constitutive activity that is countered in a healthy axon downstream of the pathway, our current model is that axon injury triggers a release of SARM1 autoinhibition, thus enabling TIR-dependent neuronal destruction (1). Whether the N terminus, SAM, or TIR domains act independently or if there is interdomain cross-talk in response to injury is unknown.

TIR domains are platforms for homodimerization as well as heterodimerization with other TIR domains (14). Enforced homodimerization of the human SARM1 TIR (HsTIR) domain stimulates rapid consumption of NAD$^+$ followed by axon degeneration and cell death (4). The capacity of dimerized SARM1 TIR to stimulate NAD$^+$ loss and cell death is unique, because dimerization of other human TIR domains does not induce axon degeneration or cell death (4, 15, 16). Hence, the TIR domain of SARM1 possesses distinct qualities that enable SARM1-dependent NAD$^+$ loss after neuronal injury. Indeed, phylogenetic

Significance

Axon degeneration is an important pathological event in multiple neurodegenerative disorders. Axon injury stimulates the prodestructive factor SARM1, leading to the precipitous loss in the metabolite NAD$^+$. Remarkably, enforcing dimerization of the Toll/interleukin receptor (TIR) domain from SARM1 is sufficient to promote NAD$^+$ loss and axon degeneration. In this study, we uncover fundamental elements within the SARM1 TIR domain responsible for this activity, including a unique motif that is highly specific to SARM1. In addition, we discover a role for the SARM1 TIR domain in injury-induced activation of the SARM1 protein, suggesting that this domain contributes to SARM1 regulation in addition to the execution of axon degeneration. These studies identify potential avenues for therapeutic intervention in SARM1-dependent axon destruction pathways.

Author contributions: D.W.S. and D.A.G. designed research; D.W.S. and D.A.G. performed research; D.W.S., D.A.G., A.D., and J.M. analyzed data; and D.W.S., D.A.G., A.D., and J.M. wrote the paper.

The authors declare no conflict of interest.

This article is a PNAS Direct Submission.

[1]To whom correspondence may be addressed. Email: jmilbrandt@wustl.edu or diantonio@wustl.edu.

This article contains supporting information online at www.pnas.org/lookup/suppl/doi:10.1073/pnas.1601506113/-/DCSupplemental.

analysis of almost 2,000 TIR domains suggests the TIR domains from human SARM1 and its orthologs are more closely related to TIR domains found in bacteria rather than other metazoans (17). Consequently, we suspected that unique motifs in the SARM1 TIR domain promote SARM1 activity in injury-induced axon degeneration.

In this study, we demonstrate that the ability of the SARM1 TIR domain to induce NAD^+ loss and neuronal death is conserved from humans to *Caenorhabditis elegans*. Using sequence homology and structural prediction, we identify putative loop motifs in the SARM1 TIR domain, including a highly conserved SARM1-specific (SS) loop motif that we show is required for SARM1 function. These motifs are required for TIR-mediated NAD^+ loss as well as axon degeneration and neuronal cell death. Finally, we identify a residue within the SARM1 TIR domain that is dispensable for TIR function but is required for injury-induced activation of SARM1, revealing the importance of interdomain cross-talk in SARM1 regulation.

Results

Dimerization of the TIR Domain from *C. elegans* TIR-1 Promotes Neuronal Cell Death. To identify elements within the SARM1 TIR domain responsible for NAD^+ loss and cell death, we first investigated whether this TIR activity is conserved in a distant SARM1 relative. The SARM1 ortholog in *C. elegans*, *tir-1*, is implicated in nonapoptotic cell death in development and motor neuron degeneration in a model of ALS (18, 19), suggesting a conserved role in neurodegeneration. However, *tir-1* regulates developmental patterning in the nervous system as well as stimulating innate immune signaling in response to pathogens (11, 20, 21), two activities that appear inconsistent with the neurodestructive properties of human SARM1. The TIR domains from SARM1 and TIR-1 are the most homologous regions of these proteins (44% identity); hence, we sought to examine whether the capacity of HsTIR to deplete NAD^+ and promote neuronal cell death is conserved in TIR-1 (CeTIR). The TIR domain of TIR-1 (amino acids 757–917) was fused to Frb/Fkbp moieties expressed in dorsal root ganglion (DRG) sensory neurons, and dimerization was stimulated with rapamycin (Fig. 1*A*). As previously reported, dimerizing HsTIR causes robust cell death beginning as early as 8 h after rapamycin addition. In neurons expressing CeTIR, rapamycin treatment also leads to cell death (Fig. 1 *B* and *C*). Cell death induced by dimerization of CeTIR is slightly delayed compared with HsTIR, becoming apparent 12 h after rapamycin addition. Similar to dimerization of HsTIR, plasma membrane blebbing preceded the ethidium homodimer nuclear labeling that signifies cell death.

The Frb/Fkbp system enables enforced heterodimerization of select TIR combinations. We investigated whether SARM1 TIRs from humans and *C. elegans* could functionally dimerize to induce

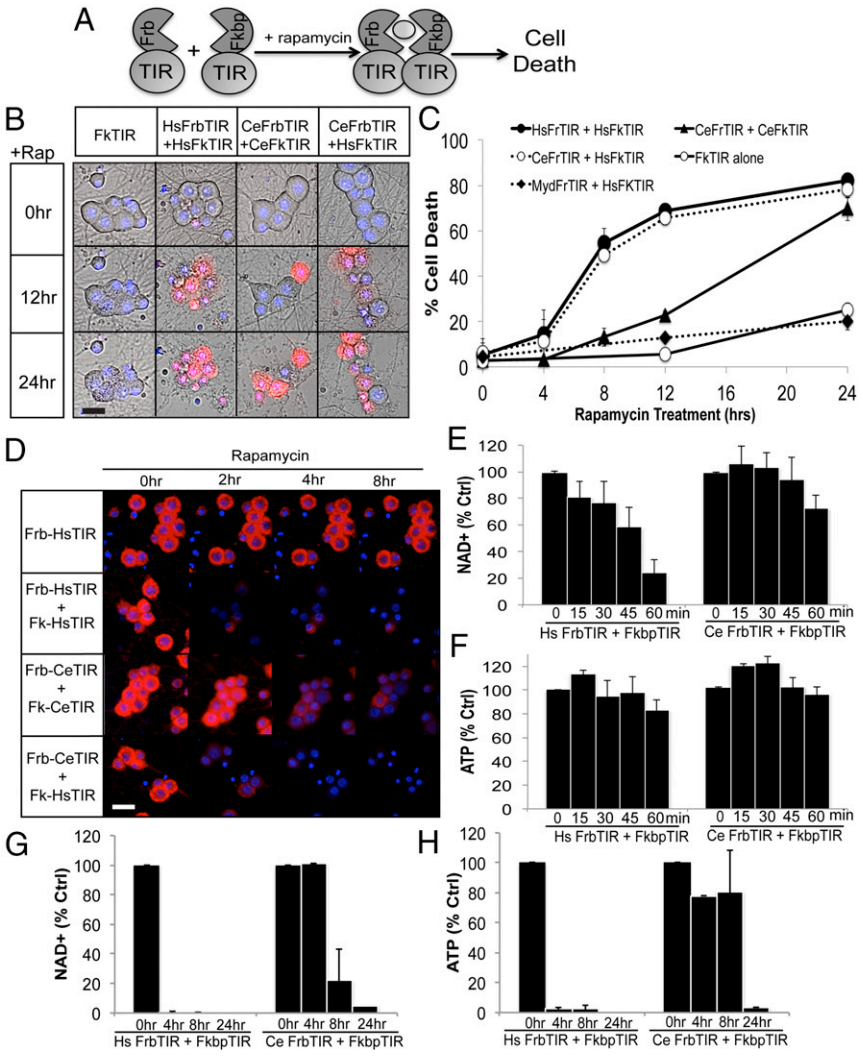

Fig. 1. Dimerization of CeTIR stimulates NAD^+ loss and neuronal cell death. (*A*) Scheme for TIR dimerization via fusing Frb and Fkbp moieties to the TIR domain. Rapamycin stimulates TIR dimerization and cell death. (*B*) Images of embryonic DRGs expressing the indicated Frb/Fkbp TIR constructs after rapamycin addition. Dying cells are labeled with ethidium homodimer and costained with Hoescht to label nuclei. (*C*) Quantification of cellular death after rapamycin addition. (*D*) $\Delta\Psi$ was monitored with tetramethylrhodamine methyl ester in DRG neurons expressing the indicated Frb/Fkbp TIR construct after rapamycin addition. (*E* and *F*) NAD^+ and ATP levels were measured from DRGs expressing the indicated Frb/Fkbp TIR construct after rapamycin addition. (*G* and *H*) NAD^+ and ATP were measured at more extended time points after rapamycin addition to assess metabolite levels after long-term TIR dimerization. Error bars reflect ± SEM (n = 3). (Scale bars, 25 μM.)

cell death. Reciprocal combinations of Frb/Fkbp TIRs were expressed in neurons and then treated with rapamycin. Human and nematode TIR heterodimers induce robust cell death with similar kinetics to HsTIR pairs (Fig. 1 *B* and *C*), indicating that exchanging one partner in the complex is sufficient to overcome the slower kinetics of CeTIR homodimers. We investigated the specificity of this phenomenon by evaluating the TIR domain from Myd88, which does not induce cell death as a homodimer (4, 15, 16). Enforced dimerization between HsTIR and the TIR domain from Myd88 did not induce cell death (Fig. 1*C*), indicating that two SARM1 TIR domains are required for functional dimerization. The finding that CeTIR forms functional dimers with HsTIR to stimulate rapid neuronal cell death is consistent with the model that the destructive function of this domain is conserved across SARM1 orthologs.

Dimerization of HsTIR leads to a precipitous drop in mitochondrial potential (ΔΨ) before cell blebbing and death (4). We investigated whether CeTIR dimerization caused a similar effect. The ΔΨ was monitored with the live-cell dye tetramethylrhodamine methyl ester. CeTIR dimerization stimulates a dramatic loss of ΔΨ ∼4 h after rapamycin treatment (Fig. 1*D*). Again, the kinetics of ΔΨ loss upon CeTIR dimerization were slightly delayed compared with HsTIR dimerization, although ΔΨ precedes the appearance of membrane blebs and labeling with ethidium homodimer as observed with HsTIR.

An important function of the HsTIR domain is its capacity to trigger rapid NAD^+ consumption upon dimerization (4). Similar to ΔΨ, NAD^+ loss precedes axon degeneration and morphological indicators of cell death by several hours. Because CeTIR dimerization stimulates neuronal cell death, we examined whether NAD^+ levels were also reduced before the detection of neuronal cell death. NAD^+ and ATP levels were measured in DRG neurons expressing HsTIR or CeTIR dimerization constructs at the indicated times after rapamycin addition (Fig. 1 *E*–*H*). In DRGs expressing HsTIRs, NAD^+ levels decline within 30 min of rapamycin treatment and have dropped over 90% by 2 h (Fig. 1 *E* and *F*). ATP levels also decline, although substantial ATP loss is observed only after NAD^+ levels are barely detectable. Within this time course, CeTIR dimerization did not trigger a change in NAD^+ or ATP. Because CeTIR dimerization stimulates death at a much later time point than HsTIR dimerization, we analyzed NAD^+ and ATP levels at later time points (Fig. 1 *G* and *H*). Indeed, NAD^+ levels begin to decrease by 4 h after rapamycin treatment and continued to decline after prolonged CeTIR dimerization. Similar to HsTIR dimerization, ATP decline is delayed compared with NAD^+, because ATP levels remain stable for up to 8 h but are largely undetectable 24 h after rapamycin addition. Hence, the capacity of HsTIR dimerization to induce energetic failure and neuronal death is conserved between humans and nematodes. This functional conservation, as well as the ability for the human and worm TIR domains to heterodimerize functionally, suggests that structural motifs that enable these unique activities are present in SARM1 and TIR-1.

The SARM1 TIR Domain Possesses a Unique Loop Motif. Conservation of the core functions of the SARM1 TIR domain encouraged us to search for sequence elements within this TIR domain that contribute to its unique activity. TIR domains are defined by a stereotypical secondary structure architecture composed of alternating β-strands and α-helices (14). Surface-exposed loop motifs between β-strand and α-helix elements are highly divergent between TIR domains and contribute to selective TIR/TIR interaction and function. For example, loop motifs called BB and DD loops (named for their adjacent β-strand and α-helix) are especially important in TIR signaling. Mutagenesis of these loops inactivates signaling of many well-studied TIR domains (22–25). However, each TIR domain uses a particular combination of motifs to mediate unique TIR/TIR interactions. As such, we sought to define canonical TIR loop motifs as well as identify unique features in the SARM1 TIR domain that might enable its specialized functions (e.g., triggering NAD^+ consumption). We used multiple structure prediction algorithms to identify the putative secondary structure architecture of the SARM1 TIR domain (Fig. 2*A*). The predicted secondary structure of the *C. elegans* TIR domain closely matches the predicted secondary structure of HsTIR. These predicted structures were compared with the structures obtained through crystallization studies of numerous TIR domains, including those TIR domains from TLR1 and Myd88 (14). Using this approach, we identified the putative BB and DD loops in the SARM1 TIR domain based on the location of these loop regions in relation to adjacent secondary structure elements. The BB loop in our analysis closely matches the sequence identified by a recent study investigating how the BB loop from the SARM1 TIR domain impacts binding to the TIR-containing adaptors Myd88 and TIR domain-containing adaptor inducing interferon beta (TRIF) (26).

We also identified a major difference between the predicted secondary structure of SARM1 TIR domains and the predicted secondary structure of other crystallized TIR domains, because we found an extended loop region between the βc and αc elements (Fig. 2*B*). Sequence alignments highlight a motif present in the TIR domain from SARM1 and its functional relative TIR-1, whereas this loop is much shorter or missing from other human TIR domains. This motif shows strong homology in diverse SARM1 orthologs with numerous amino acids highly conserved across distant SARM1 relatives (Fig. 2*C*). In contrast, the DD loop was quite divergent, with only a few amino acids showing strong conservation. Similar to the SS loop, the BB loop was extensively conserved across many SARM1 relatives.

Functional Analysis of TIR Motifs in SARM1-Dependent Axon Degeneration. Upon identifying the BB and DD loops as well as a previously unstudied TIR motif (the SS loop) in the SARM1 TIR domain, we investigated the contribution of these motifs to SARM1 function in injury-induced axon degeneration. Individual point mutations in highly conserved residues were generated in full-length human SARM1 fused with Venus at the C terminus and expressed in $SARM1^{-/-}$ neurons. The Venus tag allowed us to evaluate localization of each SARM1 mutant as well as expression levels relative to WT SARM1 (Figs. S1 and S2). Injured axons do not degenerate in SARM1-deficient neurons (2, 3). However, reexpression of human SARM1 restores injury-induced axon degeneration, thus providing an assay with which to identify important functional residues. Neurons expressing SARM1 with inactivating mutations will not undergo axon degeneration, whereas innocuous mutations will support degeneration similar to WT SARM1 (3). SARM1 mutants were expressed in $SARM1^{-/-}$ primary sensory DRGs using lentivirus infection, axons were transected, and the degeneration of distal axons was measured using an in-house–generated algorithm in which degenerated axons manifest in a score of 0.35 or higher (Fig. 2*D*). Several point mutations led to very low SARM1 expression, and these point mutations were not evaluated further (noted with asterisks in Fig. 2*C*). The SARM1 mutants shown in Fig. 2*E* have expression levels comparable to WT SARM1 and, as with WT human SARM1, localize predominantly to mitochondria and are present in axons (3) (Fig. S1). However, the precise location of endogenous SARM1 is still unclear, because pools of nonmitochondrial SARM1 are also reported (2, 3).

In the BB loop, two highly conserved charged residues (E596K and K597E) as well as a highly conserved glycine (G601P) were targeted for point mutagenesis. Individual point mutations in these residues completely abolish SARM1 activity, because axons were preserved for 24 h after axotomy (Fig. 2 *E* and *F*).

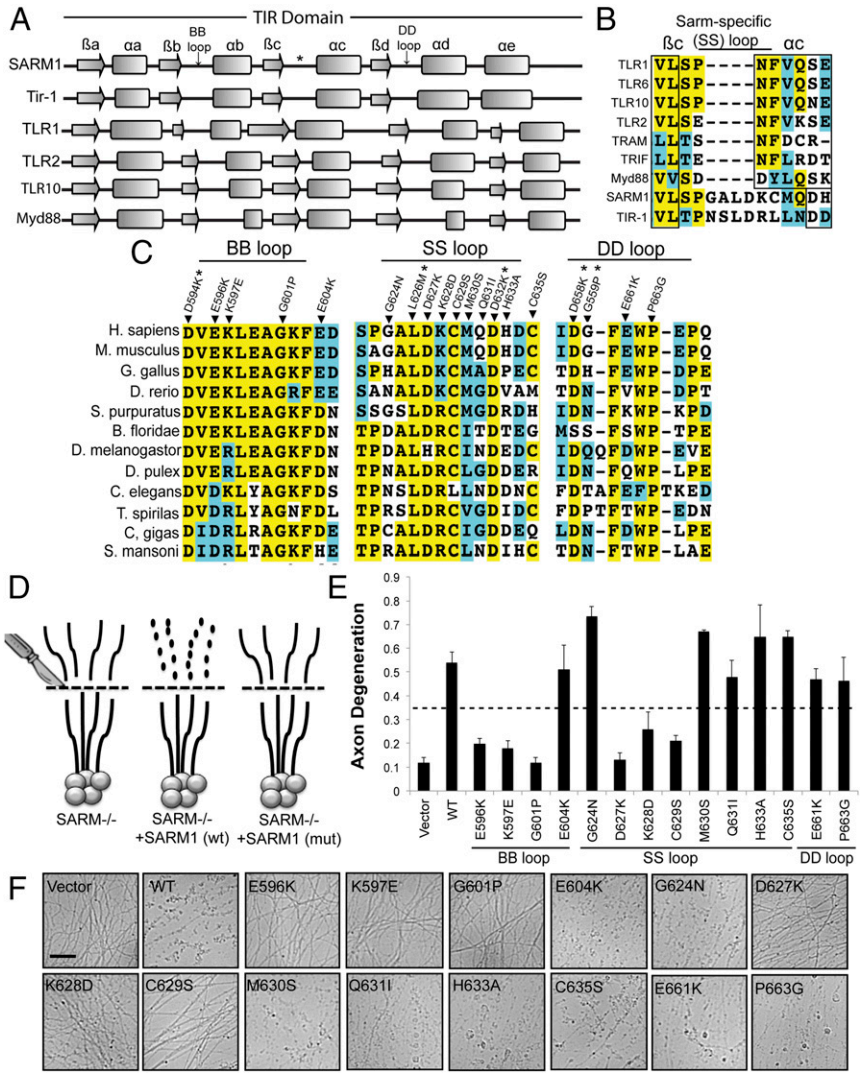

Fig. 2. Residues within the TIR domain are required for SARM1-dependent axon degeneration. (*A*) Secondary structure of TIR domains from human SARM1 and *C. elegans* TIR-1 was predicted with three algorithms. The secondary structures of other human TIR domains are shown below. Secondary structures are derived from solved crystal structures. The β-sheets and α-helices are labeled using conventional nomenclature applied to these elements in TIR domains. (*B*) Extended loop region between the βc and αc elements in the TIR domain from SARM1 and TIR-1 is largely absent in other human TIR domains. We are calling this motif the SS loop. (*C*) Sequence alignments of TIR motifs in SARM1 orthologs. Residues highlighted in yellow are conserved. Residues highlighted in blue are amino acid changes to similar residues. Residues that not highlighted are poorly conserved. Residues chosen for mutagenesis are indicated in the alignment. *SARM1-Venus expression was very low. (*D*) Diagram of rescue strategy in SARM1$^{-/-}$ DRGs. SARM1$^{-/-}$ DRGs expressing full-length SARM1 restore axon degeneration, whereas SARM1 containing loss-of-function mutations (mut) does not rescue axon degeneration. (*E* and *F*) Axons from SARM1$^{-/-}$ DRGs expressing the indicated SARM1-Venus construct were transected with a razor blade. Axon degeneration was measured 24 h later. Degenerated axons manifest in an axon degeneration score of 0.35 or greater (indicated by dashed line). Error bars reflect ± SEM ($n = 3$). (Scale bar, 25 μM.)

However, mutation of a residue outside the predicted BB loop (E604K) has no effect on SARM1 function. These observations confirm the functional importance of the BB loop to SARM1 activity.

To investigate the function of the SS loop, we performed extensive point mutagenesis of this motif targeting both highly and poorly conserved residues. Individual mutagenesis of three sequential residues (D627K, K628D, and C629S) in the middle of the SS loop strongly disrupted SARM1 function in axon degeneration (Fig. 2 *E* and *F*). Notably, these residues are particularly well conserved among SARM1 orthologs (Fig. 2*C*). Mutagenesis of adjacent residues did not affect SARM1 activity or strongly reduced SARM1 expression (e.g., L626M, D632K). These studies clearly show that residues within the SS loop are essential for the ability of SARM1 to promote axon degeneration.

The DD loop is far less conserved in SARM1 orthologs than the BB and SS loops. We mutated several residues to investigate the function of this motif (Fig. 2 *E* and *F*). Two individual point mutations disrupted SARM1 function; however, these mutants (D658K and G659P) expressed poorly. Other mutations examined did not affect SARM1 activity. Although this loop region might contribute to SARM1 activity, we are currently unable to draw concrete conclusions based on these observations, and so focus the remaining studies on the BB and SS loops.

Mutation of SARM1 Motifs Impairs TIR Activity. We identified TIR motifs that are necessary for SARM1-dependent axon degeneration in response to traumatic axon injury. These residues impact activity of full-length SARM1, and we hypothesized that these motifs would be necessary for activity of the isolated TIR domain, particularly the capacity to stimulate NAD^+ loss. To explore this hypothesis, we tested a subset of mutations described above in the homodimerizable SARM1 TIR model system (4) (Fig. 3*A*). The SARM1 TIR domain is fused to an Fkbp variant (DmrB) at the N terminus that undergoes homodimerization in the presence of a rapamycin analog (AP20187). After enforcing TIR dimerization with AP20187, we are able to monitor parameters such as NAD^+ loss, ΔΨ loss, and neuronal cell death. DmrB-TIR constructs also contained a C-terminal Venus tag to monitor expression (Fig. S3). We tested three loss-of-function mutations in the BB loop and two loss-of-function mutations in the SS loop. Wild-type SARM1 TIR stimulates neuronal cell death within 8 h of AP20187 induction. Two of three point mutations in the BB loop (E596K and G601P) and both SS loop mutations (D627K and C629S) completely block TIR-induced cell death as long as 24 h after AP20187 addition (Fig. 3*A*). As a second measure of neuronal health, we examined ΔΨ in DRGs after AP20187 addition and found that ΔΨ was also preserved after dimerization of these mutants (Fig. 3*B*).

Dimerization of the SARM1 TIR domain stimulates rapid NAD^+ loss and subsequent collapse of ATP levels. We examined whether the BB or SS loops contribute to this important SARM1 activity. NAD^+ and ATP were measured from neuronal extracts 10 h after AP20187 addition. Although NAD^+ and ATP levels are largely depleted in the presence of WT TIR, dimerization of the four TIR mutants that failed to promote cell death also failed to reduce NAD^+ or ATP levels (Fig. 3 *E* and *F*). Hence, the BB loop and the newly identified SS loop are required for TIR activity in SARM1-dependent NAD^+ destruction and axonal degeneration.

In these studies, we identified one mutant, the BB loop mutation (K597E), that stimulates cell death as effectively as the WT TIR domain (Fig. 3 *A* and *B*). This finding was surprising because full-length SARM1 containing this mutation did not support injury-induced axon degeneration when it was expressed in SARM1$^{-/-}$ neurons (Fig. 2*E*). We compared the kinetics of early morphological indicators of cell death (plasma membrane blebbing) and $\Delta\Psi$ loss between WT and K597E mutant SARM1 TIR domains. Time course analysis revealed that dimerization of mutant TIR (K597E) induced $\Delta\Psi$ loss and plasma membrane blebbing with the same kinetics as WT TIR (Fig. 3 *C* and *D*). Furthermore, dimerization of TIR (K597E) also led to NAD^+ and ATP decline (Fig. 3 *E* and *F*), demonstrating that this mutant TIR domain is equivalent to WT TIR in these assays. These results indicate that mutating this residue abolishes activity of full-length SARM1 in response to axon injury but that this residue is dispensable for TIR domain activity in an enforced dimerization assay.

SARM1 K597E Does Not Affect Toxicity of the SAM-TIR Fragment. The discovery that mutation of K597 within the SARM1 TIR BB loop abolishes the activity of full-length SARM1 but does not affect TIR activities is quite striking. This result implies that K597 might influence interdomain communication between the TIR domain and another domain in SARM1: either the SAM domains or the N-terminal autoinhibitory domain. To discriminate between these two possibilities, we investigated how the K597E mutation impacts the function of the constitutively active SAM-TIR fragment of SARM1. This fragment lacks the autoinhibitory N terminus, and its expression triggers spontaneous neuronal cell death (3, 27) (Fig. 4*A*); however, like injury-induced axon degeneration, its effects can be suppressed by the NAD^+ precursor nicotinamide riboside (NR) (4). Hence, if the K597E mutation within the TIR domain impacts SAM-dependent multimerization, then it will block SAM-TIR–mediated cell destruction. However, we found that expression of WT SAM-TIR or the mutant SAM-TIR (K597E) in DRG neurons induced cell death to a similar extent. In contrast, mutagenesis of residues in the BB loop (E596K) and SS loop (D627K) that are required for TIR function in the dimerization assay also inactivates SAM-TIR (Fig. 4 *B* and *C* and Fig. S4). To ensure that SAM-TIR (K597E) is stimulating sarmoptosis as we have previously characterized with WT SAM-TIR (4, 7), DRG neurons

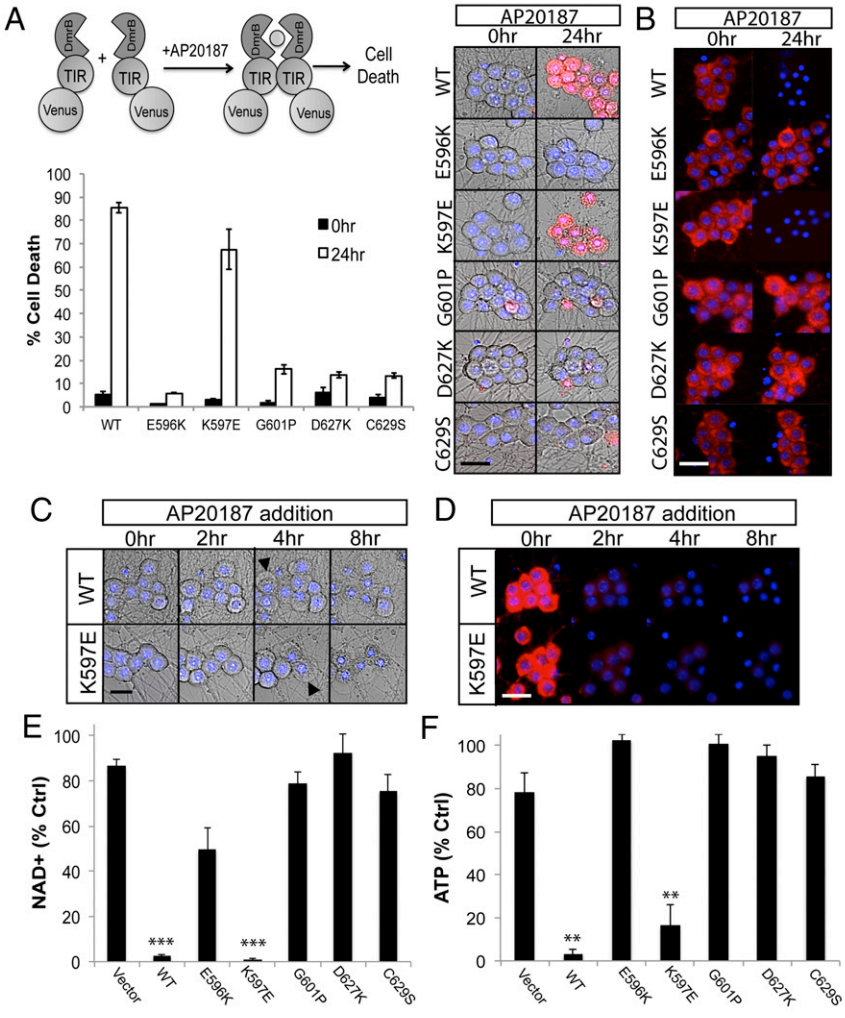

Fig. 3. Mutagenesis of TIR motifs abrogates NAD^+ loss upon TIR dimerization. (*A*) Point mutations were made in homodimerizable (DmrB) TIR, wherein AP20187 induces dimerization and neuronal death. Nonfunctional point mutations in the BB loop and SS loop prevent DmrB-TIR–dependent death 24 h after AP20187 addition. Images of ethidium homodimer-labeled DRG neurons (*Right*) and quantification (*Lower*) are shown. (*B*) Tetramethylrhodamine methyl ester is preserved in DRGs expressing loss-of-function TIR mutations 24 h after AP20187 addition. DmrB-TIR (K597E) induces cell death as well as WT, even though this mutation abolishes activity of full-length SARM1. (*C* and *D*) Kinetics of membrane blebbing and TMRM loss upon dimerization of WT TIR or K597E TIR. (*E* and *F*) NAD^+ and ATP levels are substantially reduced 10 h after AP20187 treatment in DRG cells expressing WT and K597E DmrB-TIR; however, levels are preserved in the presence of loss-of-function TIR mutants. Error bars reflect ± SEM ($n = 3$). (Scale bars, 25 μM.) $^{**}P < 0.01$.

were pretreated with NR. Similar to WT SAM-TIR, cell death triggered by SAM-TIR (K597E) was potently suppressed by NR (Fig. 4 *B* and *C* and Fig. S4). These results are consistent with our findings above in which K597E does not alter the executioner activity of the TIR domain. Furthermore, because this BB loop mutation does not impact putative interactions between the SAM and TIR domains, we suspected this residue influences activity of the N terminus.

Mutant SARM1 (K597E) Acts as a Dominant Negative and Blocks Injury-Induced Axon Degeneration. SARM1 containing a K597E mutation within the BB loop is inactive, yet fragments of SARM1 with this mutation that lacks the N-terminal domain retain full cell destructive activity. Studies from our group and others suggest that the SARM1 N terminus maintains SARM1 in an autoinhibited state until injury provokes activation of the molecule (3, 11, 12). These results suggest that the K597E TIR mutation might influence this N-terminal function. To gain further insight, we took advantage of the fact that functional SARM1 is a multimer. This requirement for multimerization is demonstrated by experiments showing that SARM1 mutants with inactivating TIR domain mutations act as dominant negatives and block axon degeneration in WT neurons (3). Because expression of the SARM1 (K597E) mutant in SARM1$^{-/-}$ neurons is unable to support injury-induced axon degeneration (Fig. 3), we explored whether it might act as a dominant negative in WT neurons. Indeed, SARM1 (K597E) expression potently inhibited axon degeneration for at least 36 h postaxotomy (Fig. 5*A*). We also examined whether the injury-induced loss in axonal ΔΨ was altered by SARM1 (K597E) expression. Twenty-four hours after transection, ΔΨ was preserved in DRG axons expressing SARM1 (K597E) (Fig. S5), indicating that the morphologically intact severed axons are metabolically active.

We explored whether SARM1 (K597E) expression could block other forms of SARM1-dependent axon degeneration and cell death. Axon degeneration in response to the chemotherapeutic agent vincristine is strongly attenuated in SARM1$^{-/-}$ axons (3). Indeed, SARM1 (K597E) expression blocked axon degeneration in response to the chemotherapeutic agent vincristine (Fig. 5*B*). Furthermore, SARM1 (K597E) expression suppressed axon degeneration and cell death after treatment with carbonyl cyanide 3-chlorophenylhydrazone (CCCP) (Fig. 5 *C* and *D*), a mitochondrial toxin that stimulates SARM1-dependent axon degeneration and cell death (7). In contrast, SARM1 (K597E) did not suppress cell death in response to trophic factor withdrawal (Fig. S6), a form of neuronal cell death that is independent of SARM1 (3).

Based on studies with the isolated TIR domain, SARM1 (K597E) is competent to deplete NAD$^+$. However, if SARM1 (K597E) cannot be activated in response to injury, then we predict that NAD$^+$/ATP levels would not plummet in transected axons from neurons expressing this mutant, because its TIR activity would still be restrained by the N terminus. To test this hypothesis, we examined axonal NAD$^+$ and ATP levels after axon transection. In SARM1$^{-/-}$ DRGs, axonal NAD$^+$ and ATP remain stable after transection and reexpression of WT SARM1 leads to a rapid decline in axonal NAD$^+$ and ATP after injury (Fig. 6 *A* and *B*). However, in the presence of SARM1 (K597E), there is no significant decrease in axonal NAD$^+$ in the transected axon within 10 h after injury. In SARM$^{-/-}$ DRGs, axonal NAD$^+$ levels eventually decline to ∼40% of control. We attribute this decrease to the loss of the NAD$^+$ biosynthetic enzyme NMNAT2, which is degraded in both WT and SARM1$^{-/-}$ neurons (28). We see robust preservation of axonal ATP levels in SARM1$^{-/-}$ DRGs expressing SARM1 (K597E), because ATP levels persist at 70% of control for 18 h after axotomy (Fig. 6*B*). Because SARM1 (K597E) expression delays axon degeneration in WT DRGs, we also examined NAD$^+$/ATP levels in transected axons from WT DRGs expressing this mutant. Overexpression of SARM1 (K597E) delays NAD$^+$ and ATP decline in WT DRGs (Fig. 6 *C* and *D*), consistent with its dominant negative activity. Intriguingly, SARM1 (K597E) expression preserves severed axons for over 36 h after injury; however, axonal NAD$^+$ levels decline to below 20% within 18 h after injury. Because ATP levels are still maintained (∼75% of uninjured axons), delaying NAD$^+$ loss is sufficient to maintain ATP levels for a prolonged period, and thus extend axon health. Such findings are consistent with other reports suggesting that NAD$^+$ must be depleted below 5% to impact cell viability (29). These observations collectively demonstrate that SARM1 (K597E) impairs injury-induced activation of the SARM1 protein and reveal a surprising link between autoinhibition and N-terminal and SARM1 TIR domains.

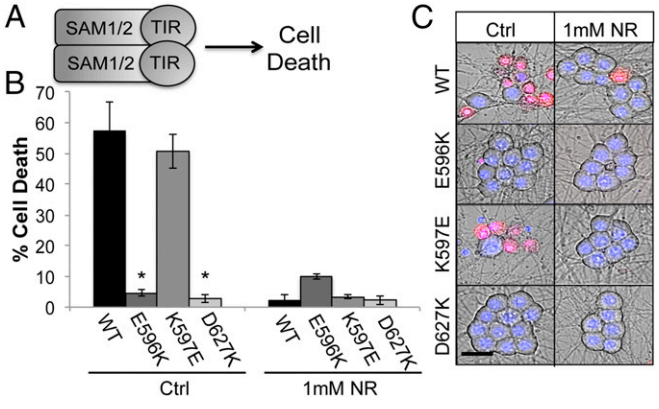

Fig. 4. K597E does not impair SAM-TIR–dependent neuronal death. (*A*) Expression of fragment containing the SAM domains and TIR domain from SARM1 induces neuronal cell death. (*B*) Quantification of neuronal death in cells expressing the indicated SAM-TIR protein. DRGs were also preincubated with 1 mM NR, which suppresses SARM1-dependent cell death. (*C*) Images of DRG neurons labeled with ethidium homodimer. *$P < 0.05$. Error bars reflect ± SEM ($n = 3$). Ctrl, control. (Scale bar, 25 μM.)

The TIR Domain Physically Interacts with the N Terminus of SARM1. The functional interaction between the SARM1 N-terminal and TIR domains described above led us to investigate whether or not these domains also have a physical interaction. The TIR domain from the cytosolic adaptor TRIF is regulated by direct physical interaction with the N-terminal domain (30), and a similar mechanism regulates activity of TIR-containing resistance proteins from plants (31). To investigate whether the SARM1 TIR and N-terminal domains are in close proximity within the full-length molecule, we used Förster resonance energy transfer (FRET), a powerful approach to investigate intramolecular interactions. FRET pairs Cerulean and Venus were fused to the N terminus and TIR domain at the C terminus of full-length SARM1, respectively (CerSARMVen). Expression of CerSARMVen rescues axon degeneration in severed SARM1$^{-/-}$ (Fig. S7), indicating that the addition of fluorescent tags did not impair function. A strong FRET signal is detected in DRG axons expressing this CerSARMVen that is comparable to a direct fusion of Cerulean and Venus alone (Fig. 7*A*). Furthermore, deletion of the TIR domain reduces FRET to background levels that are comparable to FRET obtained following the coexpression of Cerulean and Venus as separate proteins. Hence, FRET between the N and C termini of SARM1 is dependent upon the presence of the TIR domain. We did not observe a change in FRET in severed axons upon axotomy (Fig. S7), suggesting that conformational changes in activated SARM1 do not disrupt Cerulean/Venus interaction or that only a small fraction of SARM1 is activated in response to axonal injury.

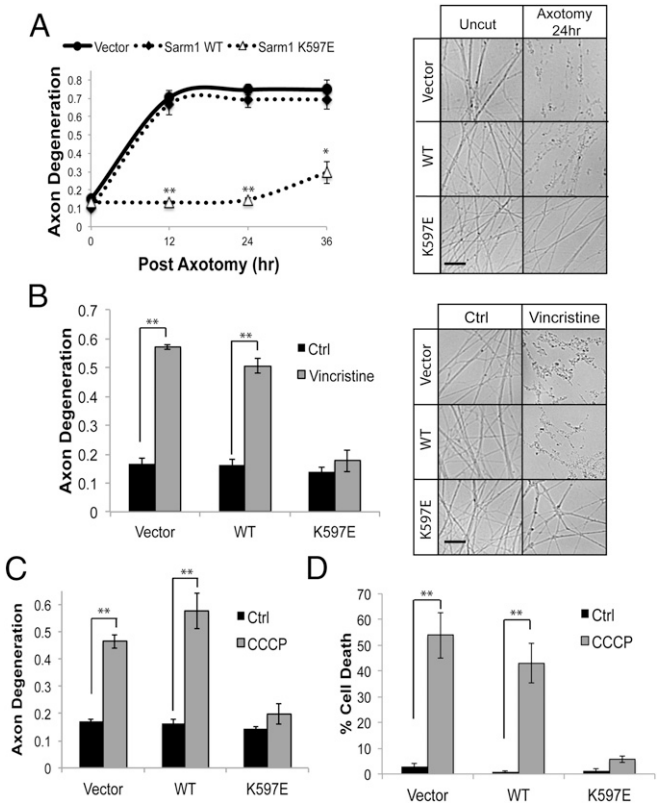

Fig. 5. Sarm1 (K597E) is a potent dominant negative, blocking axon degeneration after axotomy. (*A*) Axons from WT DRG neurons expressing the indicated Sarm1 construct were transected, and the degeneration of distal axons monitored over time. Expression of Sarm1 (K597E) delays axon degeneration for ∼36 h postaxotomy. (*B*) Expression of SARM1 (K597E) also preserves axon integrity in response to the chemotherapeutic agent vincristine. Axons were treated with 40 nM vincristine, and axon degeneration was measured 36 h postexposure. Expression of SARM1 (K597E) suppresses axon degeneration (*C*) and cell death (*D*) in response to the mitochondrial uncoupling agent CCCP (50 μM, 24 h). $*P < 0.05$; $**P < 0.01$. Error bars reflect ± SEM ($n = 3$). (Scale bars, 25 μM.)

These studies suggest the SARM1 N terminus is in close enough association to the TIR domain to elicit a FRET signal. Because the above experiment was performed in the context of full-length SARM1, we wondered whether the N terminus can physically interact with the TIR of SARM1 even when these domains are not present in the same molecule. Thus, we examined whether these fragments form a complex when expressed together *in trans*. Differentially tagged forms of the SARM1 N-terminal domain and TIR domain were expressed in HEK293T cells, and coimmunoprecipitation studies were performed. Indeed, the N terminus and TIR domain of SARM1 coimmunoprecipitate with one another, suggesting these two SARM1 domains physically interact. TIR (K597E) likewise physically associated with the N terminus (Fig. 7*B*). The association of the mutant TIR domain with the N terminus is consistent with our functional studies that showed that autoinhibition is maintained in the TIR (K597E) mutant.

Because the K597E mutation converts SARM1 into a dominant negative, we wondered if this mutation might enhance binding between the TIR domain and the N terminus in full-length, natively folded SARM1. To test this hypothesis, we used a protease-sensitive (ps) form of SARM1 that possesses a tobacco etch virus (TEV)-protease site between SAM2 and the TIR domain (4). SARM1ps is functional; however, upon TEV proteolysis, the N terminus/SAM domains are separated from the TIR domain and SARM1 is rendered inactive. Using a Cerulean tag on the C terminus, the TIR domain was immunoprecipitated from HEK293T cell extracts in the presence or absence of TEV proteolysis and the coprecipitated N terminus/SAM fragment was assessed using a SARM1 antibody generated against a peptide in the SAM2 domain. Consistent with the findings above, the SARM1 N terminus/SAM fragment coimmunoprecipitated with the TIR domain. Notably, the interaction is strongly enhanced (threefold; $P < 0.05$) in the presence of the K597E mutation in the TIR domain (Fig. 7*C* and Fig. S8). These findings support a model wherein N-terminal autoinhibition of TIR activity is mediated by direct binding between the N terminus and the TIR domain.

Discussion

SARM1 activation in response to neuronal injury evokes a rapid consumption of NAD^+ followed by a decline in ATP that ultimately leads to local axonal degeneration or neuronal cell death (4, 13). Although the molecular signaling pathways underlying SARM1-dependent neuronal destruction are still being defined, dimerization of the TIR domain of SARM1 is sufficient to stimulate NAD^+ loss and neuronal death. Our study identifies important motifs in the SARM1 TIR domain that enable SARM1-specific functions (e.g., NAD^+ loss), including a conserved loop motif that is only present in SARM1 orthologs. Furthermore, we uncover a surprising connection between the SARM1 TIR domain and autoinhibition mediated by the N terminus and provide evidence for a physical interaction between these two domains. Our studies have important mechanistic implications for SARM1 activation as well as the execution of neuronal self-destruction upon injury.

SARM1-Unique Motifs Confer TIR-Dependent Axon Degeneration. TIR domains across diverse phyla, including animals, plants, and fungi, contribute to cellular defense by stimulating innate immune signaling pathways in response to pathogens (32). SARM1 is one of five TIR-containing adaptor proteins in the cytosol, although unlike other TIR adaptors, including Myd88 or TRIF, human SARM1 inhibits innate immune signaling (33). At the sequence level, TIR domains in the SARM1 family show greater similarity to bacterial TIR domains than the TIR domains found in metazoans (17). We predicted that unique motifs within the SARM1 TIR domain would contribute to its specific functions. Structural prediction identified a loop motif that is unique to the SARM1 family that we call the SS loop. Three conserved sequential residues in the SS loop were required for SARM1 function in injury-induced axon degeneration. In particular, this motif is necessary for TIR-dependent NAD^+ loss upon TIR dimerization. We hypothesize that this motif enables SARM1-specific functions, including NAD^+ consumption, in response to axonal injury. Whether this motif is a platform for protein interaction with a downstream executioner molecule or contributes to TIR/TIR dimerization is an important question for future studies.

We also identified putative BB and DD loops in the SARM1 TIR. The BB loop contributes to TIR function in many proteins (14); in some cases, it serves as the dimerization interface in a TIR/TIR complex. The BB loop is highly conserved across distant SARM1 relatives and is essential for SARM1-dependent axon degeneration. Compared with TIR domains from other proteins, the SARM1 BB loop is largely distinct, with the exception of a highly conserved glycine (G601). Mutagenesis of this residue strongly inhibited SARM1 activity in injury-induced axon degeneration as well as TIR-dependent NAD^+ loss and death. Mutagenesis of this residue also interfered with SARM1-dependent suppression of innate immune signaling (26). Hence, the BB loop contributes to diverse SARM1 functions, potentially as an interface for TIR/TIR dimerization as seen in other TIR

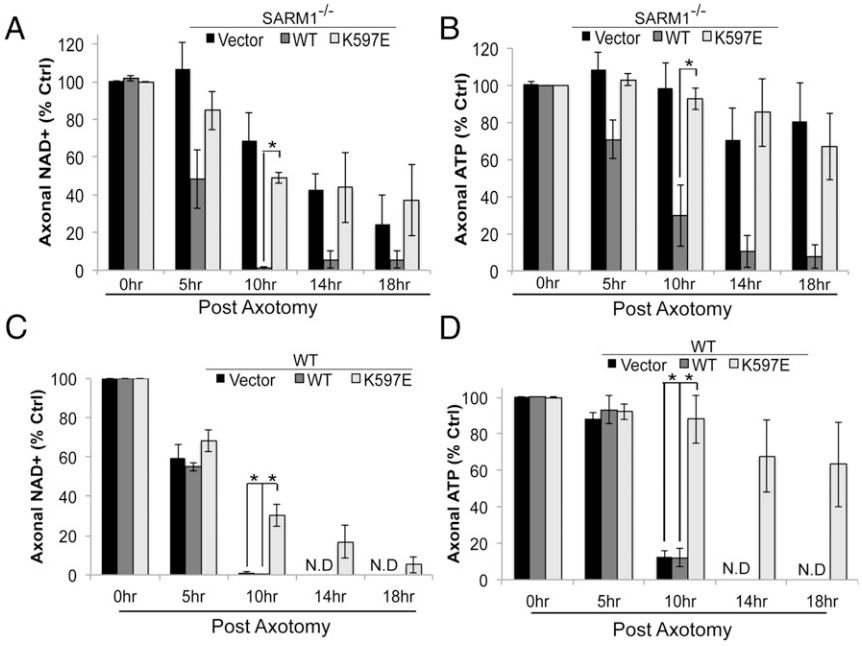

Fig. 6. SARM1 (K597E) expression prevents axonal NAD^+ loss after axotomy. (*A* and *B*) Axonal NAD^+ and ATP levels were measured from transected $SARM1^{-/-}$ DRGs expressing an empty vector, WT SARM1, or SARM1 (K597E). There is a significant drop in axonal NAD^+ in the presence of SARM1; however, there is no significant decrease in the presence of SARM1 (K597E). (*C* and *D*) Axonal NAD^+ and ATP levels were measured from transected WT DRGs expressing the same constructs as described in *A* and *B*. Expression of SARM1 (K597E) delays axonal loss of NAD^+ and ATP after axotomy. $^*P < 0.05$. Error bars reflect ± SEM ($n = 3$). N.D, not detectable.

domains. The DD loop is another prominent TIR motif that contributes to TIR/TIR interactions (23, 34, 35), but it is not highly conserved in SARM1 orthologs. In accord, our mutagenesis of the DD loop did not identify functionally important residues, suggesting that this motif contributes to SARM1 activity in a minor fashion.

The SARM1 TIR Domain Is a Conserved Executioner of Neuronal Destruction. The function of SARM1 in neurodegeneration is conserved from mammals to invertebrates (2, 3). In our study, we find that the capacity of the SARM1 TIR domain to promote neuronal cell death is also conserved in the nematode ortholog TIR-1. Furthermore, neuronal cell death is preceded by loss of $\Delta\Psi$ and NAD^+/ATP collapse. However, the prodestructive activity of TIR-1 poses a conundrum, because in a number of situations, *C. elegans tir-1* mediates nondestructive cellular signaling. For example, *tir-1* promotes survival in response to pathogenic infection by stimulating gene expression of innate immune pathways (20, 21) and participates in specification of left/right symmetry in the developing nervous system (11). In addition, axon degeneration can occur through mechanistically distinct pathways from Wallerian degeneration (36). Importantly, *tir-1* acts upstream of a MAPK signaling pathway, a function that is also conserved, because vertebrate SARM1 activates a MAPK signal during injury-induced axon degeneration (11, 13, 20, 36). Hence, both signaling and NAD^+-depleting functions of the SARM1 TIR domain are conserved. It is not known how these two activities of SARM1 TIR domains are related, or how the same molecule can promote survival signaling as well as cellular demise.

Activity of the TIR domain from TIR-1 is attenuated compared with the HsTIR. If TIR motifs such as the SS loop interact with a NAD^+ consuming enzyme, then differential kinetics of TIR-induced cell death may be due to lower affinity for potential binding partners within the mouse cellular environment. Alternatively, the SARM1 TIR domain itself might be an enzyme that directly consumes NAD^+. As such, lower activity might permit TIR-1 to carry out signaling functions without compromising cell viability. In this model, following traumatic injury, TIR-1 activity is stimulated to such an extent that it evokes cell death.

TIR Motifs Modulate Injury-Induced SARM1 Activation. Others and we previously demonstrated that deletion of the SARM1 N terminus generates a constitutively active protein (3, 11), indicating that the N terminus autoinhibits SARM1 activity in the absence of injury. Although the TIR domain is clearly important for execution of SARM1-dependent axon degeneration, we identify here a role for the SARM1 TIR domain in injury-induced activation of SARM1. Mutagenesis of Lysine597 in the SARM1 BB loop prevents SARM1 activation; however, this residue is completely dispensable for the prodegenerative activity of the dimerized TIR domain. This residue is highly conserved in SARM1 relatives, and substitutions occurring at this position in any species are limited to the similarly charged arginine. Furthermore, using the BB loop for two functions, activation and execution, would allow for direct coupling of SARM1 injury-induced activation to downstream axon destruction.

TIR-containing proteins use numerous strategies to regulate TIR/TIR interactions. For example, TLRs couple ligand binding to conformational changes that are transduced through the plasma membrane to TIR domains in the cytosol and activate signaling pathways (37). The cytosolic adaptor TRIF/TICAM1 uses a mechanism wherein the N-terminal domain folds back onto the TIR domain to hide essential effector residues in the unstructured region adjacent to the TIR domain (30). Interestingly, TIR-containing proteins in plants use a similar mechanism to suppress the activity of plant immune resistance proteins that promote cellular death (31). Our studies support a model whereby direct physical interaction between the N terminus of SARM1 with its TIR domain is necessary for SARM1 autoinhibition. We observe a strong intramolecular FRET signal between the N terminus and TIR domain in the context of full-length SARM1. These two domains also form a physical complex when expressed *in trans*. The N terminus might physically restrict TIR domains from dimerizing or block association with an auxiliary factor required for TIR activity. Interestingly, mutation of Lysine597 enhances physical association between the TIR domain and the rest of the SARM1 protein, suggesting residues in the BB loop might contribute to this physical interaction.

How axonal injury stimulates physical release of N-terminal autoinhibition is unknown. We anticipate that other residues in the SARM1 TIR domain and N terminus (and perhaps SAM domain) contribute to SARM1 regulation. Furthermore, how injury

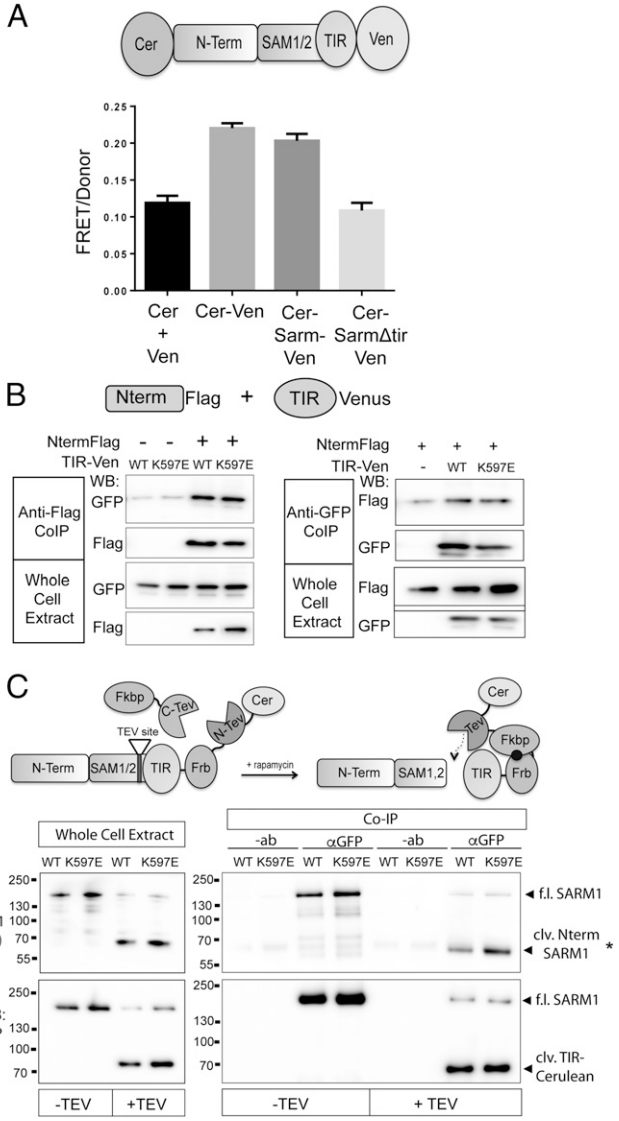

Fig. 7. SARM1 N terminus and TIR domain form a physical complex. (*A*) FRET pairs Cerulean and Venus were attached to the N terminus and C terminus of SARM1, respectively (CerSARMVen). The FRET/donor ratio in DRGs from CerSARMVen was higher than Cerulean and Venus expressed *in trans* (Cer + Ven) and comparable to a direct Cerulean-Venus fusion. Deletion of the SARM1 TIR domain reduces FRET signal to background levels. (*B*) N terminus (Nterm) of SARM1 tagged with a Flag epitope was expressed in HEK293T cells with the TIR domain (WT or K597E) tagged with Venus. Error bars reflect ± SEM ($n = 3$). TIR-Venus was immunoprecipitated from HEK293T cell extracts, and the coimmunoprecipitated Nterm was assessed by Western immunoblotting (WB) for Flag. Nterm Flag was immunoprecipitated from cell extracts, and coimmunoprecipitated TIR-Venus was assessed by Western immunoblotting for GFP. Western blots are reflective of four independent experiments. (*C*) SARM1ps was transfected in HEK293T cells with or without Fkbp-C-TEV to cleave an engineered TEV site upstream of the TIR domain. (*Left*) WB of whole-cell extracts shows efficient proteolysis to generate cleaved (clv.) Nterm SARM1 containing Nterm and SAM domains, detected with antibody that recognizes peptide in the SAM2 domain of SARM1. Proteolysis also generates a fragment containing the SARM1 TIR domain tagged with Cerulean (detected with GFP antibody). TIR-Cerulean was immunoprecipitated with GFP antisera or antibody (−ab) as a control. In the presence of Fkbp-C-TEV (+TEV), a bound SARM1 fragment containing Nterm/SAM domains is detected with anti-SARM1 antibody by Western blot (*clv. Nterm SARM1). (*Lower*) GFP WB detecting immunoprecipitated TIR-Cerulean. Western blots are representative of five independent experiments. Co-IP, coimmunoprecipitation; f.l., full length.

signals impinge on these motifs to activate SARM1 and promote its cell-destructive activities is a major outstanding question in SARM1 biology. In particular, specific injury signals might guide activity of the SARM1 TIR domain to different end points (i.e., inhibiting innate immune signaling versus inducing cell death). Elucidating how the SARM1 molecule navigates these signaling crossroads may identify novel opportunities for therapeutic intervention.

Materials and Methods

Generation of Constructs. All constructs were subcloned by InFusion (Clontech) in a lentiviral plasmid backbone described elsewhere (38). Constructs were expressed from an ubiquitin promoter. If a construct is not tagged with a fluorophore, then lentiviral transduction efficiency was monitored with a Venus driven by an internal ribosomal entry sequence. The TIR domain (amino acids 757–917) of *C. elegans* TIR-1 (designed as CeTIR) was codon-optimized for expression in the mouse and synthesized (Life Technologies). Two constructs were generated: (*i*) CeTIR was fused with an Frb moiety at the N terminus and Flag tag at the C terminus, and (*ii*) CeTIR was fused with an Fkbp moiety at the N terminus and Venus tag at the C terminus. The TIR domain of human Myd88 (amino acids 160–295) was fused with an Frb moiety at the N terminus and Venus tag at the C terminus. For studies using DmrB homodimerizable TIR, the TIR domain from human SARM1 (amino acids 559–704) was fused at the N terminus with DmrB (Clontech) and Venus at the C terminus.

Culture of Mouse Primary Embryonic DRG Neurons. Primary embryonic DRG cells were isolated from embryonic day (E) 13.5 mouse embryos as previously described (39). For rescue studies, DRGs were isolated from SARM1$^{-/-}$ embryos at stage E13.5. DRG neurons were maintained in neurobasal medium supplemented with L-glutamine (Invitrogen), 2% (vol/vol) B27 (Invitrogen), 50 ng/mL NGF (Harlan Laboratories), and 1 μM 5-fluoro-2′deoxyuridine plus 1 μM uridine (Sigma) to induce death of mitotic cells. DRG neurons were seeded on plates precoated with poly-D-lysine and laminin.

Lentiviral Transduction. Lentiviral particles were generated from HEK293T cells as previously described (38). Briefly, expression constructs for the indicated SARM1 mutant were cotransfected with plasmids containing lentiviral packaging proteins and vesicular stomatitis virus glycoprotein. After 48 h posttransfection, lentiviral particles in the media were concentrated using Lenti-X concentrator (Clontech) and resuspended in PBS. Transduction efficiency in DRGs was assessed visually by Venus fluorescence.

Analysis of Axon Degeneration and Cell Death. DRGs were spotted in 96-well plates and infected with lentivirus expressing the indicated construct on days in vitro (DIV) 1. On DIV7, axons were severed with a razor blade and axons distal to the site of injury were imaged (a 20× objective was used in all imaging experiments) using a high-content Operetta imager (PerkinElmer). Axon degeneration was quantified from bright-field images using an ImageJ macro (38) that defines the ratio of fragmented axon area to total axon area. For an individual experiment, six fields were analyzed from two to three wells per condition. For cell death analysis, DRG neurons were incubated with ethidium homodimer/Hoechst 33342 for 1 h, and cell bodies were then imaged with the Operetta imager at that indicated time point. Percentage of cell death was calculated as the ratio of ethidium homodimer-positive cells to total Hoechst-positive cells. For studies with NR (Chromadex), at least 100 cells were counted from two to three wells each per experiment. For all studies, at least three independent experiments were performed. A paired *t* test was performed to assess statistical differences between treatments.

Measurement of NAD$^+$ and ATP. DRG cultures were grown in 24-well plates and infected with lentivirus expressing the indicated protein on DIV1. Fresh media were added to the cells every 2 d. On DIV7, DRGs expressing DmrB-TIR constructs were treated with AP20187 or DMSO vehicle for 10 h. Cells were washed two times with cold PBS, and NAD$^+$/ATP was extracted using the perchloric acid/sodium carbonate method and separated with high-performance liquid chromatography as previously described (38). For experiments measuring NAD$^+$/ATP from axonal extracts, DRG axons were severed with a razor blade at the indicated time. After transection, cell bodies were physically removed from the culture dish. Axons were washed twice with cold PBS, and axonal NAD$^+$/ATP was extracted as described above.

Secondary Structure Prediction. The TIR domain from human SARM1 (amino acids 559–724) and *C. elegans* TIR-1 (amino acids 757–917) was analyzed with three separate algorithms: PsiPred, Jpred, and SABLE. The consensus secondary structure is shown in Fig. 2*A*. There was strong overlap between these three algorithms for the position of β-strands and α-helices. For comparison with

other TIR domains, the secondary structures from the following crystal structures were used: TLR1 (1FYV), TLR6 (4OM7), TLR10 (2J67), TLR2 (1FYW), TRAM (2M1W), and Myd88 (2Z5V).

Sensitized Emission FRET. Measurements of FRET intensity using the sensitized emission method were performed in live embryonic DRG neurons infected on DIV1 with lentivirus expressing the SARM1-FRET construct. Imaging was performed on DIV7 using the Operetta high-content imager. All measurements were taken from single axons. The SARM1-FRET construct consists of a cytosolic version of SARM1 (amino acids 1–27 deleted) in which the N terminus is tagged with the FRET donor mCerulean and the C-terminal TIR domain is tagged with the FRET acceptor Venus; the donor and acceptor are both attached with a short peptide linker. Images of mCerulean intensity were collected using a 430/25 excitation filter and a 470/30 emission filter, and FRET images were collected using a 430/25 excitation filter and a 525/20 emission filter. Images of neurons expressing only mCerulean were used to calculate donor bleed-through (BT) using a 430/25 excitation filter and a 525/20 emission filter. Neurons expressing only Venus imaged using a 430/25 excitation filter and a 525/20 emission filter showed no appreciable cross-excitation of Venus. The donor BT value was calculated for each experiment performed.

After background subtraction, relative FRET efficiency was determined by measuring both the mCerulean and FRET intensity in the same regions of single axons. The corrected FRET intensity was determined by subtracting the percentage of the donor signal that is BT, and thus contributes to the raw FRET intensity:

$$\mathrm{FRET}_{corrected} = \mathrm{FRET}_{raw} - \left(\mathrm{mCerulean}_{intensity} \times \mathrm{BT}\right).$$

The corrected FRET intensity value is then divided by the donor intensity value to yield the relative FRET efficiency:

$$\text{Relative FRET efficiency} = \mathrm{FRET}_{corrected}/\mathrm{Donor}.$$

All image processing and measurements for FRET experiments were performed using ImageJ (NIH).

Coimmunoprecipitation. HEK293T cells were transfected with the indicated plasmids using XtremeGene transfection reagent (Roche). Cells were washed with fresh media 24 h later. Cells were lysed 36 h posttransfection in nondenaturing lysis buffer [1× PBS, 2 mM EDTA, 10 mM Hepes (pH 7.4), 0.5% Triton X]. Cell extracts were briefly sonicated, and cell debris was collected in a pellet by centrifugation at 1,500 × *g* for 4 min. Supernatants were collected and incubated with 0.15% (wt/vol) BSA and the indicated antisera/resin, anti-GFP (Rockland Immunochemicals) or anti-Flag resin (preblocked in 1.5% (wt/vol) BSA; BioTool), overnight at 4 °C. Aliquots were saved in sample buffer as whole-cell extract samples. For GFP coimmunoprecipitation samples, Protein G agarose [preblocked in 1.5% (wt/vol) BSA] was added to the sample and incubated for another hour. Beads were washed three times with cold lysis buffer and resuspended in sample buffer. Precipitates and whole-cell extract samples were analyzed by SDS/PAGE and Western immunoblotting for the indicated proteins. For studies with SARM1ps, transfected cells were treated with 100 nM rapamycin for 3 h before cell lysis to induce SARM1ps proteolysis. Western blots were quantified with ImageJ.

ACKNOWLEDGMENTS. D.W.S. is supported by a Development Grant from the Muscular Dystrophy Association. D.A.G. is supported by the NIH under Ruth L. Kirschstein National Research Service Award NS092447 from the National Institute of Neurological Disorders and Stroke. A.D. and J.M are supported by funds from the NIH (Grants NS087632, AG013730, and NS065053).

1. Gerdts J, Summers DW, Milbrandt J, DiAntonio A (2016) Axon self-destruction: New links among SARM1, MAPKs, and NAD+ metabolism. *Neuron* 89(3):449–460.
2. Osterloh JM, et al. (2012) dSarm/Sarm1 is required for activation of an injury-induced axon death pathway. *Science* 337(6093):481–484.
3. Gerdts J, Summers DW, Sasaki Y, DiAntonio A, Milbrandt J (2013) Sarm1-mediated axon degeneration requires both SAM and TIR interactions. *J Neurosci* 33(33):13569–13580.
4. Gerdts J, Brace EJ, Sasaki Y, DiAntonio A, Milbrandt J (2015) SARM1 activation triggers axon degeneration locally via NAD$^+$ destruction. *Science* 348(6233):453–457.
5. Sasaki Y, Araki T, Milbrandt J (2006) Stimulation of nicotinamide adenine dinucleotide biosynthetic pathways delays axonal degeneration after axotomy. *J Neurosci* 26(33):8484–8491.
6. Wang J, et al. (2005) A local mechanism mediates NAD-dependent protection of axon degeneration. *J Cell Biol* 170(3):349–355.
7. Summers DW, DiAntonio A, Milbrandt J (2014) Mitochondrial dysfunction induces Sarm1-dependent cell death in sensory neurons. *J Neurosci* 34(28):9338–9350.
8. Kim Y, et al. (2007) MyD88-5 links mitochondria, microtubules, and JNK3 in neurons and regulates neuronal survival. *J Exp Med* 204(9):2063–2074.
9. Mukherjee P, Woods TA, Moore RA, Peterson KE (2013) Activation of the innate signaling molecule MAVS by bunyavirus infection upregulates the adaptor protein SARM1, leading to neuronal death. *Immunity* 38(4):705–716.
10. Mukherjee P, Winkler CW, Taylor KG, Woods TA, Nair V, et al. (2015) SARM1, not MyD88, mediates TLR7/TLR9-induced apoptosis in neurons. *J Immunol* 195(10):4913–4921.
11. Chuang CF, Bargmann CI (2005) A Toll-interleukin 1 repeat protein at the synapse specifies asymmetric odorant receptor expression via ASK1 MAPKKK signaling. *Genes Dev* 19(2):270–281.
12. Panneerselvam P, et al. (2013) T-cell death following immune activation is mediated by mitochondria-localized SARM. *Cell Death Differ* 20(3):478–489.
13. Yang J, et al. (2015) Pathological axonal death through a MAPK cascade that triggers a local energy deficit. *Cell* 160(1-2):161–176.
14. Ve T, Williams SJ, Kobe B (2015) Structure and function of Toll/interleukin-1 receptor/resistance protein (TIR) domains. *Apoptosis* 20(2):250–261.
15. Fekonja O, Benčina M, Jerala R (2012) Toll/interleukin-1 receptor domain dimers as the platform for activation and enhanced inhibition of Toll-like receptor signaling. *J Biol Chem* 287(37):30993–31002.
16. Panter G, Jerala R (2011) The ectodomain of the Toll-like receptor 4 prevents constitutive receptor activation. *J Biol Chem* 286(26):23334–23344.
17. Zhang Q, Zmasek CM, Cai X, Godzik A (2011) TIR domain-containing adaptor SARM is a late addition to the ongoing microbe-host dialog. *Dev Comp Immunol* 35(4):461–468.
18. Vériène J, Fossouo L, Parker JA (2015) Neurodegeneration in C. elegans models of ALS requires TIR-1/Sarm1 immune pathway activation in neurons. *Nat Commun* 6:7319.
19. Blum ES, Abraham MC, Yoshimura S, Lu Y, Shaham S (2012) Control of nonapoptotic developmental cell death in Caenorhabditis elegans by a polyglutamine-repeat protein. *Science* 335(6071):970–973.
20. Liberati NT, et al. (2004) Requirement for a conserved Toll/interleukin-1 resistance domain protein in the Caenorhabditis elegans immune response. *Proc Natl Acad Sci USA* 101(17):6593–6598.
21. Couillault C, et al. (2004) TLR-independent control of innate immunity in Caenorhabditis elegans by the TIR domain adaptor protein TIR-1, an ortholog of human SARM. *Nat Immunol* 5(5):488–494.
22. Xu Y, et al. (2000) Structural basis for signal transduction by the Toll/interleukin-1 receptor domains. *Nature* 408(6808):111–115.
23. Nyman T, et al. (2008) The crystal structure of the human toll-like receptor 10 cytoplasmic domain reveals a putative signaling dimer. *J Biol Chem* 283(18):11861–11865.
24. Loiarro M, et al. (2013) Mutational analysis identifies residues crucial for homodimerization of myeloid differentiation factor 88 (MyD88) and for its function in immune cells. *J Biol Chem* 288(42):30210–30222.
25. Loiarro M, et al. (2005) Peptide-mediated interference of TIR domain dimerization in MyD88 inhibits interleukin-1-dependent activation of NF-kappaB. *J Biol Chem* 280(16):15809–15814.
26. Carlsson E, Ding JL, Byrne B (2016) SARM modulates MyD88-mediated TLR activation through BB-loop dependent TIR-TIR interactions. *Biochim Biophys Acta* 1863(2):244–253.
27. Panneerselvam P, Singh LP, Ho B, Chen J, Ding JL (2012) Targeting of pro-apoptotic TLR adaptor SARM to mitochondria: Definition of the critical region and residues in the signal sequence. *Biochem J* 442(2):263–271.
28. Gilley J, Orsomando G, Nascimento-Ferreira I, Coleman MP (2015) Absence of SARM1 rescues development and survival of NMNAT2-deficient axons. *Cell Reports* 10(12):1974–1981.
29. Del Nagro C, Xiao Y, Rangell L, Reichelt M, O'Brien T (2014) Depletion of the central metabolite NAD leads to oncosis-mediated cell death. *J Biol Chem* 289(51):35182–35192.
30. Tatematsu M, et al. (2010) A molecular mechanism for Toll-IL-1 receptor domain-containing adaptor molecule-1-mediated IRF-3 activation. *J Biol Chem* 285(26):20128–20136.
31. Bernoux M, et al. (2011) Structural and functional analysis of a plant resistance protein TIR domain reveals interfaces for self-association, signaling, and autoregulation. *Cell Host Microbe* 9(3):200–211.
32. Brown J, Wang H, Hajishengallis GN, Martin M (2011) TLR-signaling networks: An integration of adaptor molecules, kinases, and cross-talk. *J Dent Res* 90(4):417–427.
33. Carty M, et al. (2006) The human adaptor SARM negatively regulates adaptor protein TRIF-dependent Toll-like receptor signaling. *Nat Immunol* 7(10):1074–1081.
34. Snyder GA, et al. (2014) Crystal structures of the Toll/Interleukin-1 receptor (TIR) domains from the Brucella protein TcpB and host adaptor TIRAP reveal mechanisms of molecular mimicry. *J Biol Chem* 289(2):669–679.
35. Bovijn C, et al. (2012) Identification of interaction sites for dimerization and adapter recruitment in Toll/interleukin-1 receptor (TIR) domain of Toll-like receptor 4. *J Biol Chem* 287(6):4088–4098.
36. Hayakawa T, et al. (2011) Regulation of anoxic death in Caenorhabditis elegans by mammalian apoptosis signal-regulating kinase (ASK) family proteins. *Genetics* 187(3):785–792.
37. Narayanan KB, Park HH (2015) Toll/interleukin-1 receptor (TIR) domain-mediated cellular signaling pathways. *Apoptosis* 20(2):196–209.
38. Sasaki Y, Vohra BP, Lund FE, Milbrandt J (2009) Nicotinamide mononucleotide adenylyl transferase-mediated axonal protection requires enzymatic activity but not increased levels of neuronal nicotinamide adenine dinucleotide. *J Neurosci* 29(17):5525–5535.
39. Gerdts J, Sasaki Y, Vohra B, Marasa J, Milbrandt J (2011) Image-based screening identifies novel roles for IkappaB kinase and glycogen synthase kinase 3 in axonal degeneration. *J Biol Chem* 286(32):28011–28018.